


# Ferromagnetism in Ti-doped ZnO thin films

Cite as: J. Appl. Phys. **117**, 17B908 (2015); <https://doi.org/10.1063/1.4917514>

Submitted: 16 September 2014 . Accepted: 12 December 2014 . Published Online: 13 April 2015

Q. Shao, C. Wang, J. A. Zapien, C. W. Leung , and A. Ruotolo



View Online



Export Citation



CrossMark

## ARTICLES YOU MAY BE INTERESTED IN

[A comprehensive review of ZnO materials and devices](#)

Journal of Applied Physics **98**, 041301 (2005); <https://doi.org/10.1063/1.1992666>

[Study of active surface defects in Ti doped ZnO nanoparticles](#)

Journal of Applied Physics **107**, 124303 (2010); <https://doi.org/10.1063/1.3432571>

[Magnetic and electric properties of transition-metal-doped ZnO films](#)

Applied Physics Letters **79**, 988 (2001); <https://doi.org/10.1063/1.1384478>

Lock-in Amplifiers  
Find out more today



 Zurich  
Instruments



## Ferromagnetism in Ti-doped ZnO thin films

Q. Shao,<sup>1</sup> C. Wang,<sup>1</sup> J. A. Zapien,<sup>1,2</sup> C. W. Leung,<sup>3</sup> and A. Ruotolo<sup>1,a)</sup>

<sup>1</sup>*Department of Physics and Materials Science and Centre for Functional Photonics, City University of Hong Kong, Kowloon, Hong Kong, China*

<sup>2</sup>*Center of Super-Diamond and Advanced Films (COSDAF), City University of Hong Kong, Kowloon, Hong Kong, China*

<sup>3</sup>*Department of Applied Physics and Materials Research Center, The Hong Kong Polytechnic University, Hung Hom, Kowloon, Hong Kong, China*

(Presented 6 November 2014; received 16 September 2014; accepted 12 December 2014; published online 13 April 2015)

We report our study on the origin of ferromagnetism in Ti-doped ZnO. A series of Ti doped ZnO films with increasing concentration of Ti dopant were grown and characterized in terms of structural, electrical, and magnetic properties. We found that Ti has a low solubility in the ZnO wurtzite structure. This favors stabilization of a large number of Zn vacancies, and theoretical calculations have shown that they can carry substantial magnetic moment. A carrier mediated exchange interaction between Zn vacancies is at the origin of the surprisingly high magnetic moment we measure in this compound. © 2015 AIP Publishing LLC. [<http://dx.doi.org/10.1063/1.4917514>]

### I. INTRODUCTION

The II-VI compound semiconductor zinc oxide (ZnO) is a typical *n*-type transparent semiconductor with a wide, direct band gap ( $E_g \sim 3.3$  eV at 300 K), and a large exciton binding energy ( $\sim 60$  meV). Currently employed in a broad range of applications, from solar cells and light emitting diodes (LEDs) to transparent conductive contacts and thin film transistors,<sup>1</sup> it has recently renewed much interest as a potential candidate for memristive devices.<sup>2-4</sup> Doping ZnO with 3*d* transition metals opens up new possibilities to meet the requirement of next generation multifunctional devices. The possibility of room temperature magnetism by diluting with 3*d* magnetic ions<sup>5,6</sup> makes this oxide of interest for spintronics<sup>7</sup> and magneto-optics.<sup>8</sup>

Diluting metal ions into ZnO provides an effective method to engineer electrical and magnetic properties. Compared to other 3*d* transition metals, titanium (Ti) owns several merits. Ti replaces  $Zn^{2+}$  in valence 4+, therefore provides more than one electron in the conduction band. This allows increasing the conductivity by using a lower concentration of dopant as compared to other transition metals. Diluted magnetic ZnO has been at the origin of a long lasting debate, because the magnetic signal could come from the clustering or secondary phases of the magnetic dopant.<sup>9-11</sup> Magnetism detected in ZnO doped with nonmagnetic elements, like Lithium<sup>12</sup> or Ti,<sup>13</sup> provides a strong argument against this possibility. While the solubility of magnetic dopants, such as cobalt and manganese (Mn), in ZnO has been widely investigated and proved to be relatively large,<sup>13,14</sup> the solubility of Ti into ZnO has not received much attention. Moreover, since magnetism in these compounds is carried mediated and Ti provides more carriers than magnetic transition ions in the ZnO lattice, it is interesting to understand how the magnetic moment shown by Ti-doped ZnO

compares with that of Mn-, Co-, and Ni-ZnO with dopant concentration being equal.

In the present work, we have prepared a series of Ti (0.2, 0.5, 1.0, and 2.0 at. %) doped ZnO films grown on (001) sapphire substrates by using pulsed laser deposition (PLD). The influence of the Ti dopant on the crystal structure as well as on the electrical and magnetic properties was investigated systematically. We could detect traces of TiO<sub>2</sub> in the x-ray diffraction (XRD) patterns, in both targets and films, already at 2 at. % Ti doping, which suggests a very low solubility of Ti in ZnO. Consistently, the conductivity increases with Ti concentration, but no further increase is detected when Ti starts precipitating in TiO<sub>2</sub>. We measure a surprisingly high magnetic moment and coercivity of the single-phase films as compared to magnetic-metal doped ZnO.

### II. EXPERIMENT

All single phase dense Ti doped ZnO targets (nominal 0.2, 0.5, 1.0, and 2.0 at. % Ti) were prepared via a conventional solid state reaction.<sup>4</sup> Briefly, the precursor highly pure ZnO powder (99.999% from Aldrich) and TiO<sub>2</sub> (99.99% from Aldrich) were mixed according to the desired atomic ratio. The powders were grinded by ball milling for 10 h to reduce the particles size to nano as well as to obtain a uniform mix of the elements. Subsequently, the powder was compressed by an oil-compressor at a pressure of 15 Torr. Finally, the ceramic targets were annealed at 600 °C for 12 h and later 1000 °C for 12 h.

Thin films were deposited from the sintered targets on (001) Sapphire substrates by using PLD. During the PLD deposition, a pulsed KrF excimer laser ( $\lambda = 247$  nm) with an energy of 300 mJ operated at a repetition rate of 5 Hz. The oxygen pressure in the chamber during growth was 0.1 mbar. The substrate was kept at 460 °C. All the films were grown under the same conditions, regardless Ti doping concentration,

<sup>a)</sup>Author to whom correspondence should be addressed. Electronic mail: [aruotolo@cityu.edu.hk](mailto:aruotolo@cityu.edu.hk).

and had a thickness of  $\sim 50$  nm, as estimated by Atomic Force Microscope (AFM).

The crystal structure of target and films were investigated by XRD using a Philips X'Pert with Cu  $K\alpha$  radiation source ( $\lambda_{Cu} = 0.15406$  nm). The stoichiometry of both targets and films was checked by energy-dispersive X-ray spectroscopy (EDS). EDS was also used to exclude contamination by unintentional dopants. The surface morphology was studied by using an AFM. Electrical characterization was carried out by measuring the four-point sheet resistance in magnetic field. The hysteresis loops of the grown films were measured by a Lake Shore vibrating sample magnetometer (VSM). The hysteresis loops shown in the following were corrected by subtracting the measured linear contribution of the substrate. X-ray photoemission spectroscopy (XPS) measurements were carried out with a 1486.6 eV Al K $\alpha$  source. For photoluminescence (PL) measurements, the excitation source was the fourth harmonic of a Nb:yttrium-aluminum-garnet laser and the light emission was detected using a 0.5 m spectrometer.

### III. RESULTS AND DISCUSSION

The XRD patterns of the four sintered targets, namely, 0.2, 0.5, 1.0, and 2.0 at. % Ti-doped ZnO are shown in Fig. 1(a). The x-ray intensity was collected from  $2\theta = 20^\circ - 80^\circ$ . All the patterns can be indexed by the wurtzite structure of ZnO (JCPDS Card No. 36-1451). We detect two small additional peaks in the case of 2 at. % Ti doped ZnO target, which can be indexed by the rutile structure of TiO<sub>2</sub> (JCPDS Card No. 21-1276). This means that for the target synthesis technique we used here, which is a standard solid state reaction synthesis, solubility of Ti in ZnO is limited to concentrations smaller than 2 at. %.

We verified that Ti replaces Zn with valence 4+, as theoretically expected, and by resorting to XPS on the 0.5 at. % Ti doped ZnO film. The double spectral lines of Ti 2p<sub>3/2</sub> and Ti 2p<sub>1/2</sub> are shown in Fig. 1 (inset). The peaks positions, located at 458.8 eV and 464.5 eV, respectively, match very well with those expected for Ti<sup>4+</sup> in tetrahedral coordination.<sup>15</sup>

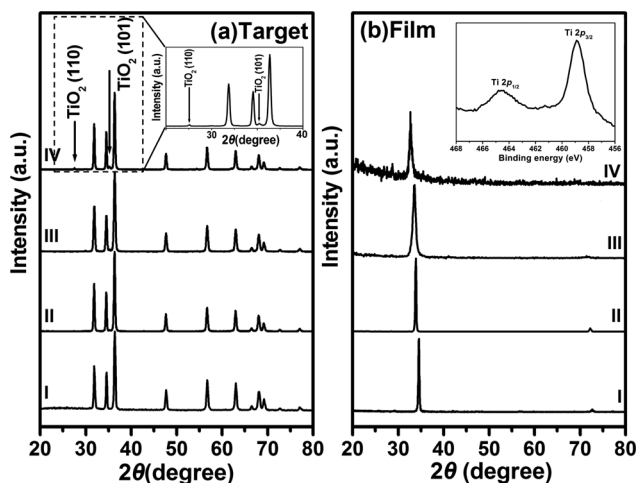


FIG. 1. XRD patterns of (a) targets and (b) films with four different Ti concentrations: I: 0.2%; II: 0.5%; III: 1.0%; and IV: 2.0%. Inset shows the XPS Ti spectrum of the film II.

Fig. 1(b) shows the XRD patterns of the Ti doped ZnO thin films, deposited under the same conditions from the respective targets. The intensity of each pattern was normalized to the respective maximum value for sake of clarity. The low signal to noise ratio in the case of the 2% Ti-ZnO film clearly highlights a much worse structural order as compared to the other three films. In the first three Ti (0.2%, 0.5%, and 1.0%) doped thin films, no detectable secondary phases were observed, suggesting that the Ti was replacing Zn into the ZnO lattice. Yet, an unexpected shift of the ZnO (002) peak position towards smaller angles can be observed as the Ti concentration increases. With the sapphire (001) peak as a reference, the (002) peaks of the Ti (0.2%, 0.5%, and 1.0%) doped thin films were located at  $34.32^\circ$ ,  $33.9^\circ$ , and  $33.66^\circ$ , respectively, where the same peak for pure bulk ZnO is expected to be at  $2\theta = 34.42^\circ$ . Since the Ti replaces the Zn in valence 4+ and the atomic radius of Ti<sup>4+</sup> is smaller than that of Zn<sup>2+</sup> (Pauling radii 0.068 nm and 0.074 nm, respectively), a shift towards larger angles was expected. The shift towards smaller angles suggests that interstitial Ti is present even in the films with very low concentration. The concentration of interstitial Ti might be too small to be detected by XRD or XPS, yet, given the large radius of the Ti atom (0.187 nm); the presence of interstitial Ti well explains the detected shift towards smaller angles. Consistently, the XRD peaks become broader as the Ti concentration increases, indicating a reduction of grain size due to additional grain boundaries originated from the interstitial Ti. The percentage of interstitial Ti in the 2%Ti-doped ZnO becomes large enough to result in the formation of a TiO<sub>2</sub> secondary phase. In fact, a small but detectable peak at  $\sim 28^\circ$  can be observed in the XRD pattern of 2%Ti-ZnO in Fig. 1(b).

In order to exclude a contribution to the magnetic moment due to surface effects,<sup>16,17</sup> it is important to verify that the films have very small and comparable surface roughness. Fig. 2 shows a typical AFM scan of our films. All the films showed a surface roughness of 0.4 nm, as estimated on a  $10 \times 10 \mu\text{m}^2$  scanning area. We can therefore exclude a significant contribution to the magnetic moment arising from the surface.

Magnetism in *n*-type diluted ZnO is carrier mediated, regardless the origin of the localized magnetic spin. Ferromagnetic exchange between neighboring localized spins is mediated by the carriers spin, with the formation of

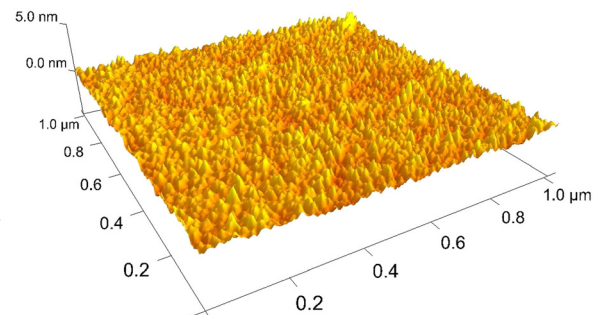


FIG. 2. XPS spectra of the O 1s peaks recorded from a 0.5 at. % Ti doped ZnO film at room temperature.

TABLE I. Hall measurement of Ti doped ZnO films with different dopant concentrations. Pure ZnO is added for reference.

| Hall parameters                     | Different dopant concentrations |                        |                        |                        |                        |
|-------------------------------------|---------------------------------|------------------------|------------------------|------------------------|------------------------|
|                                     | 0.0%                            | 0.2%                   | 0.5%                   | 1.0%                   | 2.0%                   |
| Conductivity (S/cm)                 | $2.578 \times 10^{-6}$          | $6.955 \times 10^{-6}$ | $1.755 \times 10^{-5}$ | $2.208 \times 10^{-5}$ | $1.433 \times 10^{-5}$ |
| Carrier density ( $1/\text{cm}^3$ ) | $5.328 \times 10^{16}$          | $1.975 \times 10^{17}$ | $5.638 \times 10^{17}$ | $1.383 \times 10^{18}$ | $8.148 \times 10^{17}$ |

magnetic polarons.<sup>5</sup> It is therefore important to carry out a detailed electric characterization of the samples. We measured the Hall conductivity in van der Pauw geometry in order to determine the majority carrier type and the carrier density. All measured films show n-type behavior. Table I lists the conductivity and corresponding calculated carrier density of the films with different dopant concentrations.

As expected, the carrier density increases with the Ti concentration except for the case of 2%Ti-ZnO. This is because the additional Ti precipitates into  $\text{TiO}_2$ , in agreement with the XRD. It is important to understand that the Ti is not the only dopant. A native dopant is always present in ZnO, which is represented by the oxygen vacancies ( $\text{V}_\text{O}$ 's). Both Ti and  $\text{V}_\text{O}$  are double donors and transfer two electrons in the conduction band. What we report in Table I is therefore the total carrier density. While it is hard to estimate and even harder to tune, the concentration of  $\text{V}_\text{O}$ 's in the film, it must be pointed out that our films are grown under the same temperature and oxygen partial pressure. Therefore, the concentration of  $\text{V}_\text{O}$ 's should be the same. In order to confirm it, we carried XPS measurements. The O 1s peak, shown in Fig. 3, presents three spectral contributions that were successfully disentangled by fitting analysis, resulting in three nearly Gaussian components. The strongest  $\text{O}_\text{a}$  peak of the O 1s spectrum is attributed to the Zn-O bonds in ZnO lattice, while the  $\text{O}_\text{b}$  peak at medium binding energy is attributed to  $\text{O}^{2-}$  ions in the oxygen deficient regions and the weakest  $\text{O}_\text{c}$  peak concerns surface chemisorbed or dissociated oxygen or OH species such as adsorbed  $\text{O}_2$ .<sup>18,19</sup> The ratio of the  $\text{O}_\text{a}/\text{O}_\text{b}$  is the same, within experimental accuracy, for all the concentrations of Ti dopant up to 1%, confirming a similar concentration of oxygen vacancies in the films. The increase of

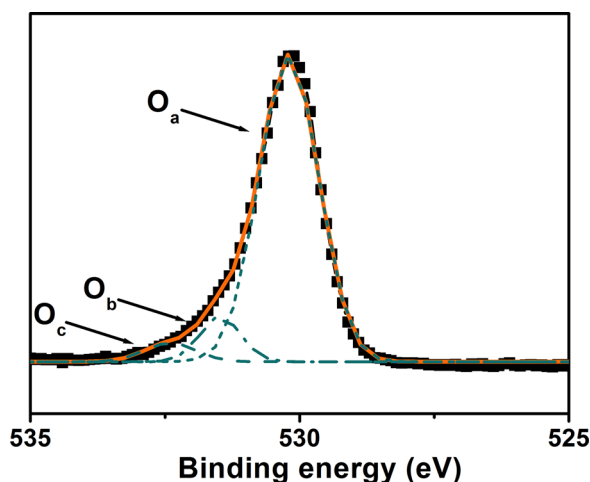


FIG. 3. AFM profile of a film of 1 at. % Ti doped ZnO.

carrier density in Table I is due to the increase of Ti dopant. This increase is linear for Ti up to 1%. This indicates that if interstitial Ti is present in the film, the fraction of it must be very small, and therefore cannot significantly contribute to the magnetic moment.

Fig. 4 shows the magnetization loop of a 1 at. % Ti doped ZnO film, recorded at 300 K and 100 K. The saturation magnetization was measured to be  $M_\text{S}$  (100 K) = 30  $\text{emu}/\text{cm}^3$  and  $M_\text{S}$  (300 K) = 11  $\text{emu}/\text{cm}^3$ , corresponding to a magnetic moment of 3.8  $\mu_\text{B}/\text{Ti}$  and 1.3  $\mu_\text{B}/\text{Ti}$ , respectively. The coercive field is about 100 Oe at 300 K and increases to 233 Oe when the temperature is lowered to 100 K. The magnetic moment is surprisingly high. It is significantly higher than that reported by Venkatesan *et al.*<sup>13</sup> and Antony *et al.*<sup>20</sup> (0.15  $\mu_\text{B}/\text{Ti}$  at room temperature in 5% Ti-ZnO) and consistent with that reported by Yong *et al.*<sup>21</sup> (0.82  $\mu_\text{B}/\text{Ti}$  at room temperature in 0.6% Ti-ZnO). To put these numbers in perspective, let us compare the magnetic moment of these films with that measured in our Mn-doped ZnO films grown in the same vacuum chamber and measured in the same magnetometer.<sup>8,21,22</sup> In Mn-doped ZnO with concentration of Mn as high as 8% and similar carrier density, we measure a magnetic moment of only 0.35  $\mu_\text{B}/\text{Mn}$  at low temperatures.

The physical origin of the magnetic moment in Mn-ZnO and Ti-ZnO must be completely different. In Mn-doped ZnO indirect exchange interaction between the magnetic Mn ions is mediated by the carrier spin. More precisely, the  $\text{V}_\text{O}$ 's form a donor impurity band that partially overlaps with the  $\text{Mn}^{2+}$  energy levels. The formation of bound magnetic polarons is due to delocalization of electrons from the impurity band to the Mn sites. This scenario is not reasonable for the

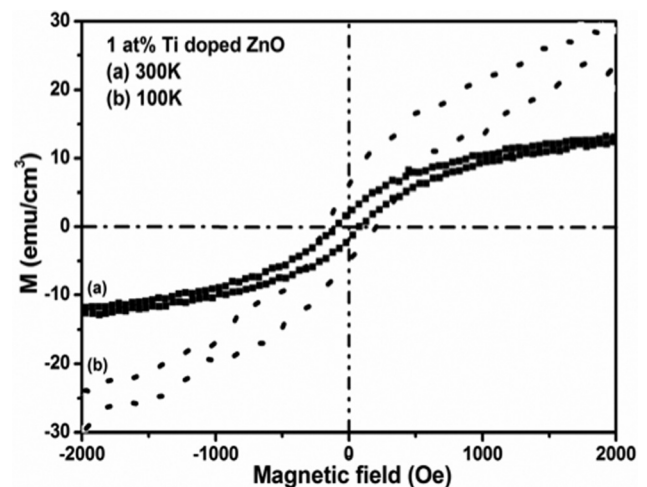


FIG. 4. Magnetization loop of a 1 at. % Ti doped ZnO film recorded at 300 K and 100 K.

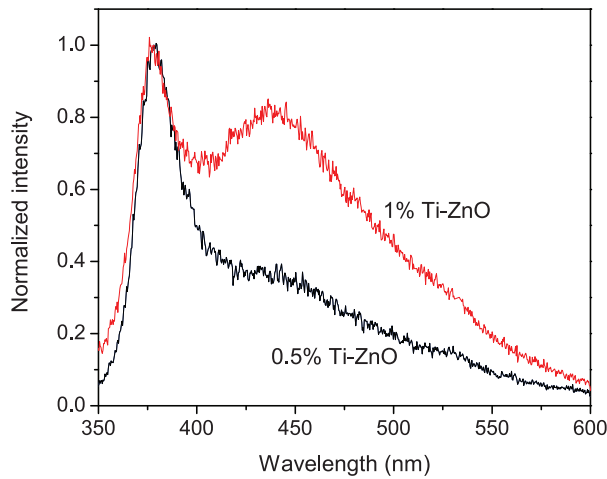


FIG. 5. PL spectra of 0.5 and 1 at. % Ti doped ZnO films recorded at room temperature.

case of Ti-ZnO.  $\text{Ti}^{4+}$  has a theoretical zero magnetic moment ( $\text{Ti} = [\text{Ar}] 3d^2 4s^2$ ). Even assuming that some of the Ti is in valence other than  $4+$ , still the  $\text{Mn}^{2+}$  has the maximum theoretical moment ( $5 \mu_B/\text{ion}$ ). Therefore, Mn-ZnO should be much more magnetic than Ti-ZnO, if the physical mechanism were the same. This strong magnetic moment is most likely due to a large presence of Zn vacancies ( $V_{\text{Zn}}$ ). Earlier works<sup>12,23,24</sup> have shown that  $V_{\text{Zn}}$ 's in ZnO prefers a spin polarized state and each  $V_{\text{Zn}}$  carries a theoretically calculated magnetic moment of  $1.3 \mu_B$  at room temperature. The role of the Ti is twofold. First, the Ti stabilizes a large number of  $V_{\text{Zn}}$ 's, in agreement with its low solubility. Second, the Ti is a real dopant and increases the concentration of carriers, which mediate exchange. The magnetic moment is the result of the exchange interaction between  $V_{\text{Zn}}$ 's mediated by the carriers spin.

In order to support this scenario, we compared the concentration of  $V_{\text{Zn}}$ 's in 0.5 and 1.0 at. % Ti doped ZnO films by resorting to PL. In ZnO films, deep level transitions between shallow donors ( $V_{\text{O}}$ 's) and deep acceptors ( $V_{\text{Zn}}$ 's)<sup>25,26</sup> can be observed, if significant, because they produce luminescence peaks in the visible band. In Fig. 5, a visible emission in the violet can be observed, which becomes very strong in the case of 1 at. % Ti doped ZnO. This emission can be ascribed to  $V_{\text{Zn}}-V_{\text{O}}$  acceptor-donor pairs.<sup>25,26</sup>

Let us finally point out that calculating the magnetic moment as  $\mu_B/\text{Ti}$  is misleading and is the reason why it might appear surprisingly high. The magnetic moment should be calculated as  $\mu_B/V_{\text{Zn}}$ , since  $V_{\text{Zn}}$  is the source of localized spin. We and other authors report it as  $\mu_B/\text{Ti}$  for the difficulty to quantitatively estimate the concentration of  $V_{\text{Zn}}$ .

#### IV. CONCLUSION

We investigated the origin of the magnetic moment in Ti-doped ZnO. A systematic characterization on thin films of Ti-doped ZnO with different concentrations of Ti dopant was carried out. XRD and Hall measurements showed that substitution of Ti in the ZnO lattice is challenging. Interstitial Ti atoms are detected in the wurtzite structure

even at very low concentration of Ti. Precipitation of a  $\text{TiO}_2$  secondary phase occurs for Ti concentration as small as 2%. This low solubility, yet, favors the stabilization of a large number of Zn vacancies, as confirmed by PL spectra, which carry a magnetic moment of  $1.3 \mu_B$ . A carrier mediated exchange interaction between Zn vacancies is at the origin of the surprisingly high magnetic moment in this compound.

#### ACKNOWLEDGMENTS

The work described in this paper was supported by the Research Grants Council of the Hong Kong Special Administrative Region, China (CityU 104512) and by the National Science Foundation of China (NSFC) (Grant No. 11274261). Financial support from CityU (7004197) is also acknowledged.

- <sup>1</sup>L. Schmidt-Mende and J. L. MacManus-Driscoll, *Mater. Today* **10**, 40 (2007).
- <sup>2</sup>H. Y. Peng, G. P. Li, J. Y. Ye, Z. P. Wei, Z. Zhang, D. D. Wang, G. Z. Xing, and T. Wu, *Appl. Phys. Lett.* **96**, 192113 (2010).
- <sup>3</sup>X. L. Wang, Q. Shao, C. W. Leung, R. Lortz, and A. Ruotolo, *Appl. Phys. Lett.* **104**, 062409 (2014).
- <sup>4</sup>X. L. Wang, Q. Shao, C. W. Leung, and A. Ruotolo, *J. Appl. Phys.* **113**, 17C301 (2013).
- <sup>5</sup>J. M. D. Coey, M. Venkatesan, and C. B. Fitzgerald, *Nat. Mater.* **4**, 173 (2005).
- <sup>6</sup>T. Dietl, H. Ohno, F. Matsukura, J. Cibert, and D. Ferrand, *Science* **287**, 1019 (2000).
- <sup>7</sup>K. M. Whitaker, M. Raskin, G. Kiliani, K. Beha, S. T. Ochsenbein, N. Janssen, M. Fonin, U. Ruediger, A. Leitenstorfer, D. R. Gamelin, and R. Bratschkis, *Nano Lett.* **11**, 3355 (2011).
- <sup>8</sup>X. L. Wang, C. Y. Luan, Q. Shao, A. Pruna, C. W. Leung, R. Lortz, J. A. Zapien, and A. Ruotolo, *Appl. Phys. Lett.* **102**, 102112 (2013).
- <sup>9</sup>P. Sharma, A. Gupta, K. V. Rao, F. J. Owens, R. Sharma, R. Ahuja, J. M. O. Guillen, B. Johansson, and G. A. Gehring, *Nat. Mater.* **2**, 673 (2003).
- <sup>10</sup>X. L. Wang, K. H. Lai, and A. Ruotolo, *J. Alloys Compd.* **542**, 147 (2012).
- <sup>11</sup>D. C. Kundaliya, S. B. Ogale, S. E. Lofland, S. Dhar, C. J. Metting, S. R. Shinde, Z. Ma, B. Varughese, K. V. Ramanujachary, L. Salamanca-Riba, and T. Venkatesan, *Nat. Mater.* **3**, 709 (2004).
- <sup>12</sup>J. B. Yi, C. C. Lim, G. Z. Xing, H. M. Fan, L. H. Van, S. L. Huang, K. S. Yang, X. L. Huang, X. B. Qin, B. Y. Wang, T. Wu, L. Wang, H. T. Zhang, X. Y. Gao, T. Liu, A. T. S. Wee, Y. P. Feng, and J. Ding, *Phys. Rev. Lett.* **104**, 137201 (2010).
- <sup>13</sup>M. Venkatesan, C. B. Fitzgerald, J. G. Lunney, and J. M. D. Coey, *Phys. Rev. Lett.* **93**, 177206 (2004).
- <sup>14</sup>T. Fukumura, Z. Jin, A. Ohtomo, H. Koinuma, and M. Kawasaki, *Appl. Phys. Lett.* **75**, 3366 (1999).
- <sup>15</sup>R. Knut, R. Lindblad, S. Grachev, J.-Y. Faou, M. Gorgoi, H. Rensmo, E. Sondergard, and O. Karis, *J. Appl. Phys.* **115**, 043714 (2014).
- <sup>16</sup>K. Sato and H. Katayama-Yoshida, *Jpn. J. Appl. Phys., Part 2* **40**, L334 (2001).
- <sup>17</sup>M. A. Garcia, J. M. Merino, and E. Fernandez, *Nano Lett.* **7**, 1489 (2007).
- <sup>18</sup>M. Chen, X. Wang, Y. H. Yu, Z. L. Pei, X. D. Bai, C. Sun, R. F. Huang, and L. S. Wen, *Appl. Surf. Sci.* **158**, 134 (2000).
- <sup>19</sup>S. Major, S. Kumar, M. Bhatnagar, and K. L. Chopra, *Appl. Phys. Lett.* **49**, 394 (1986).
- <sup>20</sup>J. Antony, S. Pendyala, D. E. McCready, and M. H. Engelhard, *IEEE Trans. Magn.* **42**, 2697 (2006).
- <sup>21</sup>Z. H. Yong, T. Liu, T. Uruga, H. Tanida, D. C. Qi, A. Rusydi, and A. T. S. Wee, *Materials* **3**, 3642 (2010).
- <sup>22</sup>Q. Shao, P. S. Ku, X. L. Wang, W. F. Cheng, J. A. Zapien, C. W. Leung, F. Borgatti, A. Gambardella, V. Dediu, R. Ciprian, and A. Ruotolo, *J. Appl. Phys.* **115**, 153902 (2014).
- <sup>23</sup>D. Galland and A. Herve, *Phys. Lett. A* **33**, 1 (1970).
- <sup>24</sup>Q. Wang, Q. Sun, G. Chen, Y. Kawazoe, and P. Jena, *Phys. Rev. B* **77**, 205411 (2008).
- <sup>25</sup>H.-J. Egelhaaf and D. Oelkrug, *J. Cryst. Growth* **161**, 190 (1996).
- <sup>26</sup>B. J. Jin, S. Im, and S. Lee, *Thin Solid Films* **366**, 107 (2000).